doi: 10.4149/gpb_2024048

Co-delivery of circCDR1 and temozolomide with hyaluronic acid-chitosan nanoparticles inhibits glioma progression

Changjiu Tang[1,*], Ye Wan[1,*], Xiaomin Zhang[1], Bao Zhong[1] and Ming Zhang[1]

[1] *Department of Neurosurgery, Jingmen People's Hospital/Jingchu University of Technology Affiliated Central Hospital, Jingmen City, Hubei, China*

Abstract. Chemotherapeutic drug/gene nanoparticles (NPs) co-delivery system has great potential in tumor therapy. However, the role of circular RNA (circRNA) cerebellar degeneration-related 1 (CDR1) (circCDR1) and temozolomide (TMZ) NPs in the treatment of glioma remains unclear. circCDR1 was significantly low expressed in glioma tissues and cells. In the term of mechanism, circCDR1 could sponge miR-890 to regulate GJB6. The inhibition of circCDR1 on glioma progression could be reversed by miR-890, and the suppressive effect of miR-890 inhibitor on glioma progression also could be overturned by GJB6 silencing. CNPs could introduce TMZ and circCDR1 into glioma cells. The inhibitory effects of CNPs on glioma cell progression and tumor growth were much better than TMZ, TNPs and CNPs. Our study showed that circCDR1 could regulate the miR-890/GJB6 axis to inhibit glioma progression, and the constructed CNPs had a good inhibitory effect on glioma progression.

Key words: Glioma — Nanoparticles — circCDR1 — Temozolomide — miR-890 — GJB6

Introduction

Glioma is the most common central nervous system tumor in neurosurgery, mainly caused by abnormal proliferation of glial cells in the brain (Ostrom et al. 2015; Ferris et al. 2017). Due to the characteristics of invasive growth, glioma is difficult to treat and recurs easily, so it is one of the tumors with the worst prognosis in the whole body (Lv et al. 2018; Mair et al. 2018). Therefore, finding effective treatments is of great significance to improve the survival of glioma patients.

Circular RNA (circRNA) is a type of non-coding RNA molecule that forms a circular structure with covalent bonds, and has high stability in organisms (Chen and Yang 2015; Barrett and Salzman 2016). The competitive endogenous RNA (ceRNA) hypothesis reveals that circRNA has the ability to competitively bind with microRNA (miRNA), thereby reducing the inhibitory effect of miRNA on its downstream target (Thomson and Dinger 2016; Zhang et al. 2019). A large number of studies have confirmed that circRNA is involved in the tumorigenesis process and has the potential to become a biomarker for tumor treatment and diagnosis (Li et al. 2019; Zhao et al. 2019). Circ_0001946 (derived from cerebellar degeneration-related 1 (CDR1) gene, also called circCDR1) has been found to be a significantly down-regulated circRNA in glioblastoma and may be a potential therapeutic target for glioblastoma (Li et al. 2019). Therefore, more mechanisms related to circCDR1 in glioma should be Zhangfurther explored.

At present, tumor-targeted therapy based on new nanotechnology has become a hot research area in tumor treat-

Electronic supplementary material. The online version of this article (doi: 10.4149/gpb_2024048) contains Supplementary material.

* These authors contributed equally to this paper.

Correspondence to: Xiaomin Zhang, Department of Neurosurgery, Jingmen People's Hospital/Jingchu University of Technology Affiliated Central Hospital, Building 22, Xishan Linyu, Dongbao District, Jingmen City, 448000, Hubei Province, China
E-mail: dreams4641@163.com

Changjiu Tang, Department of Neurosurgery, Jingmen People's Hospital/Jingchu University of Technology Affiliated Central Hospital, Building 22, Xishan Linyu, Dongbao District, Jingmen City, 448000, Hubei Province, China
E-mail: tangchangjiu2023@126.com

© The Authors 2025. This is an **open access** article under the terms of the Creative Commons Attribution-NonCommercial 4.0 International License (https://creativecommons.org/licenses/by-nc/4.0/), which permits non-commercial use, distribution, and reproduction in any medium, provided the original work is properly cited.

ment (Hu et al. 2017). Nanoparticles (NPs), as a new type of chemotherapeutic drug/gene co-carrier, have gradually demonstrated their application potential in tumor treatment (Yang and Gao 2017; Zang et al. 2017). Compared with traditional chemotherapy, the chemotherapeutic drug/gene NPs co-carrier method can reduce the dosage of chemotherapy drugs and increase the distribution of drugs in target organs, so as to reduce toxic side effects and improve curative effects (Kang et al. 2015; Li et al. 2016). Therefore, the chemotherapeutic drug/gene NPs co-carrier system will play an important role in the treatment of cancer in the future. Hyaluronic acid (HA) is a polymer mucopolysaccharide that can specifically interact with the tumor cell surface receptor CD44 to achieve the purpose of identifying tumor cells (Chiesa et al. 2018; Cai et al. 2019). Chitosan (CS) is a positively charged polysaccharide macromolecule with good biocompatibility and biodegradability, which has been widely studied as a drug carrier (Assa et al. 2017; Zhang et al. 2019). Since CS has a large number of positive charges and HA has a negative charge, the two can form poly ion nanocomposite through non-covalent interaction. By taking advantage of the cationic nature of CS, gene delivery can be carried out, and HA has the specific targeting function of tumors. At present, HA-CS NPs has shown great advantages in chemotherapy drug and gene delivery (Deng et al. 2014; Almutairi et al. 2019).

In this study, we also explored the new mechanism of circCDR1 regulating the progression of glioma through the hypothesis of the circRNA/miRNA/mRNA axis. In addition, HA-CS NPs were used to deliver the chemotherapy drugs temozolomide (TMZ) and circCDR1 to achieve the co-delivery of chemotherapy drugs and gene. By exploring the impact of different types of NPs on the progression of glioma, the advantages of the chemotherapy drug/gene NPs co-delivery system in glioma were evaluated. Our research aims to provide new evidence for the treatment of glioma with drugs/genes NPs co-delivery system.

Materials and Methods

Samples collection

In this study, 41 patients with glioma were recruited from Jingmen People's Hospital/Jingchu University of Technology Affiliated Central Hospital and their glioma tumor tissues were collected after surgery. Patients were followed up for 5 years thereafter. In addition, the brain tissues from 10 patients undergoing intracranial decompression surgery at the same hospital were collected as healthy controls. All patients signed informed consents. Our study was approved by the Ethics Committee of Jingmen People's Hospital/Jingchu University of Technology Affiliated Central Hospital.

Cell culture and transfection

Human glioma cells (U251 and LN229) and normal astrocytes cells (NHA) were obtained from Procell Life Science & Technology Co., Ltd. (Wuhan, China). All cells were cultured in DMEM medium (Gibco, Grand Island, NJ, USA) supplemented with 10% fetal bovine serum (FBS; Gibco) and 1% Penicillin-Streptomycin solution (Sangon Biotech, Shanghai, China) at 37°C with 5% CO_2. Cell transfection was performed using Lipofectamine 3000 (Invitrogen, Carlsbad, CA, USA). All oligonucleotides and vectors were synthesized by Ribobio (Guangzhou, China), including pCD5 circCDR1 overexpression vector (circCDR1) or its negative control (pCD5-ciR), miR-890 mimic and inhibitor (miR-890 and in-miR-890) or their negative controls (miR-con and in-miR-con), as well as Gap junction beta 6 (GJB6) small interfering RNA (siRNA) (si-GJB6) and its negative control (si-con).

Quantitative real-time PCR (qRT-PCR)

TRIzol reagent (Invitrogen) was used to extract total RNA, and QuantiTect Reverse Transcription Kit (Qiagen, Düsseldorf, Germany) was utilized for obtaining cDNA. qRT-PCR was performed using the SYBR Premix Ex Taq Reagent Kit (Takara, Tokyo, Japan) on PCR system. In this, β-actin or U6 was used as the internal reference. The primer sequences were listed as below: circCDR1: F, 5'-CCAGTCTTCCATCAACTGGCT-3', R, 5'-GCCATCGGAAACCCTGGATA-3'; linear-CDR1: F, 5'-CAACACCAGGGAAACTTATCG-3', R, 5'-TCTCGCAACACCATACCTCA-3'; miR-890: F, 5'-GCTTGGAAAGGCATCAGTTG-3', R, 5'-CTCAACTGGTGTCGTGGAGTC-3'; GJB6: F, 5'-CAAGAGGACTTCGTCTGCAAC-3', R, 5'-GTGGTTTCGTGCCTGTAGTAG-3'; β-actin: F, 5'-AGCGAGCATCCCCCAAAGTT-3', R, 5'-GGGCACGAAGGCTCATCATT-3'; U6: F, 5'-CTCGCTTCGGCAGCACA-3', R, 5'-AACGCTTCACGAATTTGCGT-3'. The $2^{-\Delta\Delta Ct}$ method was used to quantify relative level.

Subcellular localization analysis

The cytoplasm RNA and nucleus RNA of U251 and LN229 cells were obtained using Cytoplasmic & Nuclear RNA Purification Kit (Norgen Biotek, Thorold, ON, Canada). Then, β-actin and U6 were used as cytoplasm and nuclear references to detect the expression distribution of circCDR1 in cytoplasm and nuclear RNA by qRT-PCR.

RNase R assay

The RNAs extracted from U251 and LN229 cells were incubated with RNase R (RNase R^+; Epicentre, Madison,

WI, USA) for 30 min. The RNA non-incubated with RNase R was used as control (RNase R^-). The expression levels of circCDR1 and linear-CDR1 were detected by qRT-PCR.

Dual-luciferase reporter assay

The fragments of circCDR1 and GJB6 3'UTR harboring miR-890 matched binding sites (wild-type, WT) or mutate sites (mutate-type, MUT) were individually inserted into pmirGLO reporter vectors (Promega, Madison, WI, USA). The generated reporter vectors were transfected into 293T cells (Procell Life Science & Technology Co., Ltd.) with miR-890 mimic or miR-con for 48 h. Luciferase activities were determined using the Dual-Lucy Assay Kit (Solarbio, Beijing, China).

RNA immunoprecipitation (RIP) assay

According to the EZ Magna RIP Kit (Millipore, Billerica, MA, USA), U251 and LN229 cells were lysed with RIP lysis buffer, and then the cell lysates were incubated with magnetic beads bounded with Anti-Ago2 or Anti-IgG antibody. The immunoprecipitated RNA was extracted for qRT-PCR to detect the enrichments of circCDR1, miR-890 and GJB6.

RNA pull-down assay

Biotin-labeled miR-890 wild-type probe (Bio-miR-890-WT) and corresponding mutate-type probe (Bio-miR-890-MUT), as well as negative probe (Bio-miR-con) were obtained from Sangon Biotech. U251 and LN229 cells were transfected with the above probes for 48 h. Then, the cells were lysed and the cell lysates were incubated with Streptavidin agarose beads (GlpBio, Shanghai, China) for 4 h. After that, the biotin-conjugated RNA was extracted and the enrichments of circCDR1 and GJB6 were detected by qRT-PCR.

Western blot (WB) analysis

Total protein was extracted using RIPA lysate (Beyotime, Shanghai, China). The protein samples were then electrophoresed by SDS-PAGE gel and subsequently transferred to PVDF membranes (Millipore). The membrane was blocked with skimmed milk for 2 h, and then incubated with the primary antibody against BCL2 (1:2000, Abcam, Cambridge, MA, USA), BCL2 Asociated X (BAX, 1:1000, Abcam), GJB6 (1:1000, Abcam) or β-actin (1:1000, Abcam) overnight at 4°C, followed by incubating with Goat Anti-Rabbit IgG H&L (1:50000, Abcam) for 2 h. ECL Chemiluminescence Development Kit (Solarbio) was used for visualizing the protein signals.

Cell counting kit 8 (CCK8) assay

U251 and LN229 cells were seeded in 96-well plates and cultured for 48 h. Then, 10 μl CCK8 reagent (Solarbio) was added into cells. After the cells were further incubated in the dark for 2 h, the absorbance at 450 nm was measured on a microplate reader (BioTek, Winooski, VT, USA) to evaluate cell viability.

Transwell assay

For detecting cell migration ability, 24-well Transwell chambers (8 μm; Corning Inc., Corning, MA, USA) were used. For measuring cell invasion ability, the top of 24-well Transwell chambers was pre-coated with Matrigel (Corning Inc.). Briefly, U251 and LN229 cells suspended DMEM medium were seeded into the top chamber. The medium containing 10% FBS was added in the bottom chamber. 24 h later, the migration and invasion cells were fixed with 4% paraformaldehyde (Beyotime) and stained with crystal violet (Beyotime). The migration and invasion cell numbers were counted under a microscope (Leica, Wetzlar, Germany) at 100× magnification.

Flow cytometry

Annexin V-FITC Apoptosis Detection Kit (Sigma-Aldrich, St. Louts, MO, USA) was used for measuring cell apoptosis. U251 and LN229 cells were digested and then mixed with AnnexinV-FITC Binding Buffer. After stained with AnnexinV-FITC solution and propidium iodide in the dark for 10 min, the apoptotic rate of cells was analyzed by flow cytometer (BD Biosciences, San Jose, CA, USA).

Construction of HA-CS NPs

Blank HA-CS NPs (BNPs): HA solution (1.25 mg/ml; Dongyuan Biotech, Zhenjiang, China) and sodium polyphosphate (TPP) solution (0.5 mg/ml; Sigma-Aldrich) were mixed to prepare HA-TPP working solution. Under the condition of magnetic stirring, the HA-TPP working solution (1 ml) was incubated with the CS solution (0.6125 mg/ml; Aoxing Biotech, Taizhou, China) for 10 min. After stabling at room temperature for 20 min, the solution was centrifuged at 3000×*g* for 10 min to remove the supernatant. Finally, the precipitate was freeze-dried to obtain BNPs.

TMZ-loaded HA-CS NPs (TNPs): The CS solution was pre-added with 0.125 mg of TMZ (Medchem Express, Monmouth Junction, NJ, USA) with the weight ratio of TMZ to CS of 1:10. The rest of the operation steps were consistent with the construction of BNPs.

CircCDR1-loaded HA-CS NPs (circNPs): Carboxyfluorescein-labeled circCDR1 (FAM-circCDR1, 20 μg; synthesized by Ribobio, Guangzhou, China) was dissolved in 100 μl of RNase-free water (Solarbio), and then added to the HA-TPP working solution (1 ml) in advance. The rest of the operation steps were consistent with the construction of BNPs.

TMZ-circCDR1 co-loaded HA-CS NPs (CNPs): FAM-circCDR1 (20 μg) dissolved in RNase-free water (100 μl) was added into the HA-TPP working solution (1 ml), and TMZ (0.125 mg) was added into the CS solution with the weight ratio of TMZ to CS of 1:10. Then, FAM-circCDR1/HA-TPP solution was incubated with the TMZ/CS solution for 10 min under the condition of magnetic stirring. After stabling at room temperature for 20 min, the solution was centrifuged at 3000×*g* for 10 min to remove the supernatant. Finally, the precipitate was freeze-dried to obtain CNPs.

Transmission electron microscopy (TEM)

The HA-CS NPs were diluted with RNase-free water (Solarbio) to 0.1 mg/ml, and then 10 μl sample was dropped on a copper mesh (230 mesh) containing a carbon support film. After drying, the sample was stained with 2% uranyl acetate for 5 min. Finally, the morphology and size of HA-CS NPs were observed with a transmission electron microscope (JEOL, Tokyo, Japan). All the materials were bought from Beijing Zhongjingkeyi Technology Co., Ltd. (Beijing, China).

Agarose gel electrophoresis analysis

According to the instructions of One-Stop RNA Electrophoresis Pack Kit (Baiaolaibo, Beijing, China), agarose (1.2 g) and ultrapure water (87 ml) were mixed. After heating and melting, the mixed solution was added with 10 ml of RNAep. After cooling to 60°C, formaldehyde solution (3 ml) and ethidium bromide (5 μl) were added into the gel solution. After shaking and mixing, the gel solution was poured into the mold to solidify for half an hour. CNPs (15 μl) and glycerol (5 μl) were mixed, and the equal amounts of circCDR1 and blank BNPs were used as controls. In addition, 15 μl CNPs were mixed with 5 μl 12% sodium dodecyl sulfonate (SDS; Sigma-Aldrich). All the samples were added to the prepared agarose gel for electrolysis (110 V, 15 min).

Laser confocal microscopy

U251 and LN229 cells were seeded in a special laser confocal culture dish overnight and divided into 3 groups. One group was added with the constructed BNPs, one group was added with the constructed CNPs, and the other group was added with 10 mg/ml HA in advance 3 h before adding the CNPs. After culturing for 3 h, the cells were fixed with 4% paraformaldehyde (Beyotime) and stained with DAPI Staining Solution (Beyotime). Use a laser confocal microscope (Leica), the distribution of TMZ (red fluorescence) and FAM-circCDR1 (green fluorescence) in U251 and LN229 cells were observed.

Glioma xenograft tumors

All animal studies were approved by the Animal Ethics Committee of Jingmen People's Hospital/Jingchu University of Technology Affiliated Central Hospital. Thirty BALB/c nude mice (6-week-olds; Vital River, Beijing, China) were subcutaneously injected in the right back with 4×10^6 LN229 cells. When the cells grew around 100 mm^3, the mice were randomly divided into 5 groups ($n = 6$ *per* group): Control group, injected with saline; circNPs group, injected with circNPs (2 mg/kg); TMZ group, injected with TMZ (5 mg/kg); TNPs group, injected with TNPs (5 mg/kg); CNPs group, injected with CNPs (containing 2 mg/kg circCDR1 and 5 mg/kg TMZ). Mice were administrated daily through the tail vein. Tumor width and length were measured every 7 days to calculate tumor volume (length×$width^2$/2). After 28 days, the mice were then sacrificed to collect all tumor tissues. Tumor tissue was photographed and weighted for further testing.

Immunohistochemistry (IHC) staining

Mice tumor tissues were dewaxed after paraffin section. After sealing with goat serum (Beyotime), the tissue sections were incubated with primary antibody against GJB6 (1:1,000, Abcam) overnight. Then, the tissue sections were incubated with Goat Anti-Rabbit IgG H&L (1:20,000, Abcam) for 2 h, and then developed with DAB (Sigma-Aldrich) for 10 min and washed with distilled water for 10 min. After the tissue sections were sealed with neutral resin (Solarbio), the immunostaining images were analyzed with a microscope (Leica).

Statistical analysis

Data from 3 independent experiments were presented as the mean ± standard deviation. Comparisons among groups were performed using Student's *t*-test or analysis of variance (ANOVA) followed by Tukey's *post hoc* test. Kaplan-Meier analysis was used to assess the relationship between circCDR1 expression and the overall survival rate of patients. The correlations were reflected by Pearson correlation analysis. Statistical analysis was conducted using the GraphPad Prism 5.0 software (GraphPad, La Jolla, CA, USA). $p < 0.05$ was considered as statistically significant.

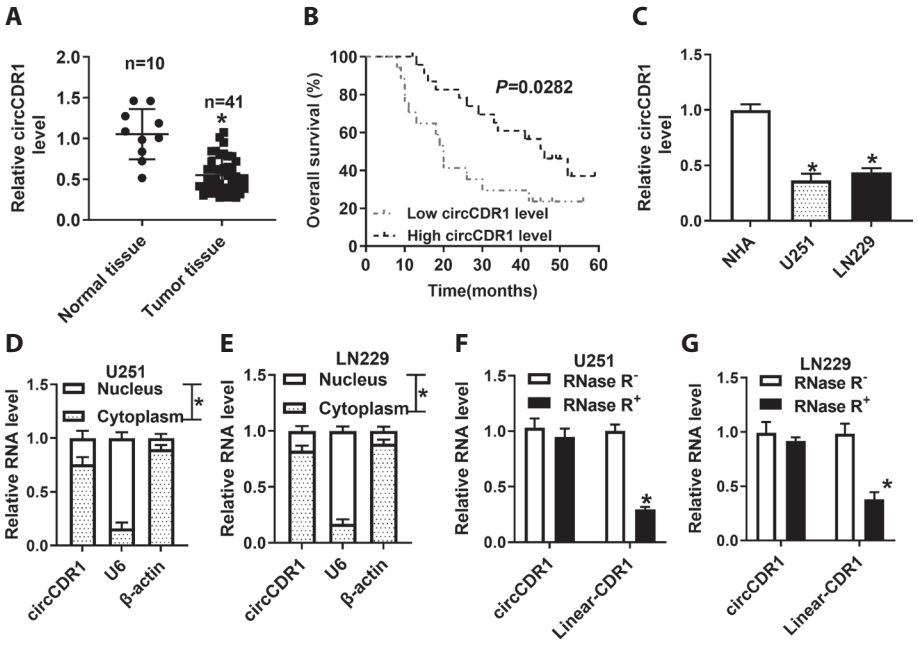

Figure 1. circCDR1 was lowly expressed in glioma tumor tissues and cells. **A.** The expression of circCDR1 in glioma tumor tissues and normal tissues was detected by qRT-PCR. **B.** Kaplan-Meier analysis was used to analyze the relationship between circCDR2 level and the overall survival of glioma patients. **C.** QRT-PCR was used to measure the expression of circCDR1 in glioma cells (U251 and LN229) and NHA cells. **D, E.** Subcellular localization analysis was employed to confirm the distribution of circCDR1 in the nuclear and cytoplasm of glioma cells. **F, G.** RNase R assay was employed to analyze the stability of circCDR1. A, Student's *t*-test; C, one-way ANOVA followed by Tukey's *post hoc* test; D–G, two-way ANOVA followed by Tukey's *post hoc* test. * $p < 0.05$.

Results

circCDR1 was lowly expressed in glioma tumor tissues and cells

In the tumor tissues of glioma, circCDR1 expression was discovered to be downregulated compared with that in normal tissues (Fig. 1A). According to the median value of circCDR1 expression in glioma tumor tissues, glioma patients were divided into high circCDR1 level group and low circCDR1 level group. Kaplan-Meier analysis showed that the overall survival rate of patients with low circCDR1 level was significantly lower than that of patients with high circCDR1 level (Fig. 1B). Moreover, circCDR1 also was markedly decreased in glioma cells (U251 and LN229) compared NHA cells (Fig. 1C). Subcellular localization analysis showed that circCDR1 was mainly distributed in the cytoplasm (Fig. 1D,E), suggesting that circCDR1 might be mainly involved in post-transcriptional regulation. In addition, circCDR1 could resistant the digestion of RNase R compared to linear-CDR1 (Fig. 1F,G), indicating that circCDR1 was more stable than linear-CDR1.

circCDR1 sponged miR-890 and miR-890 targeted GJB6

To illuminate the mechanism of circCDR1 in glioma, the circular RNA Interactome (https://circinteractome.nia.nih.gov/) was used to predict the targeted miRNA of circCDR1. Among the top 10 miRNAs, 4 miRNAs (miR-7-5p, miR-620, miR-1299, and miR-1231) were reported to be lowly expressed, while 6 miRNAs (miR-671-5p, miR-619, miR-576-3p, miR-890, miR-490-5p and miR-1246) were highly expressed in glioma tissues. We screened the highly expressed miRNAs and found that circCDR1 had

Table 1. GSE50161 database showed the top 10 genes with low expression in glioma tissues

ID	adj.*p*.Val	*p*.Value	t	B	logFC	Gene.symbol
231771_at	1.01E−12	3.17E−15	−11.555815	24.505125	−8.8424537	GJB6
227053_at	1.00E−10	1.08E−12	−9.68294	18.772271	−8.0075126	PACSIN1
205551_at	6.73E−11	6.23E−13	−9.852706	19.310708	−7.8541634	SV2B
210040_at	1.15E−10	1.26E−12	−9.635242	18.620351	−7.8332486	SLC12A5
205626_s_at	5.97E−09	1.64E−10	−8.164882	13.811499	−7.8291547	CALB1
235468_at	6.27E−13	1.67E−15	−11.772201	25.137251	−7.7307844	RBFOX3
1568612_at	5.12E−10	7.71E−12	−9.079551	16.830447	−7.6839041	GABRG2
203797_at	4.97E−09	1.32E−10	−8.229811	14.028433	−7.5693736	VSNL1
230303_at	6.02E−10	9.72E−12	−9.009111	16.601018	−7.4548271	SYNPR

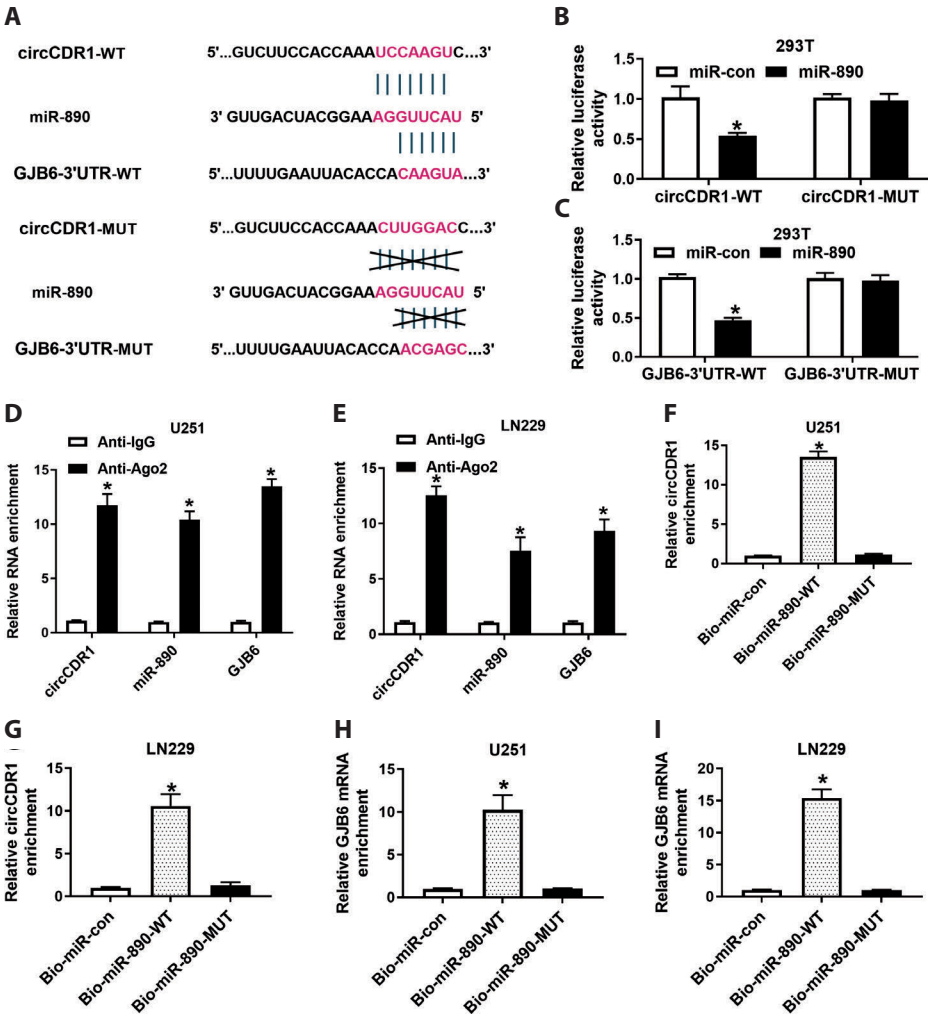

Figure 2. circCDR1 sponged miR-890 and miR-890 targeted GJB6. **A.** The binding sites and mutate sites between miR-890 and circCDR1 or GJB6 3'UTR were shown. Dual-luciferase reporter assay (**B, C**), RIP assay (**D, E**) and RNA pull-down assay (**F–I**) were used to evaluate the interaction between miR-890 and circCDR1 or GJB6. B–E, two-way ANOVA followed by Tukey's *post hoc* test; F–I, one-way ANOVA followed by Tukey's *post hoc* test. * $p < 0.05$.

the strongest inhibitory effect on miR-890 expression (Fig. S1A,B in Supplementary material). Therefore, miR-890 was selected as the target of circCDR1 for investigation. Using the GSE50161 database, we analyzed genes with low expression in glioma tissues, and GJB6 score was the highest (Table 1). In addition, among the top 5 genes, microT CDS software (http://diana.imis.athena-innovation.gr/DianaTools/index.php?r=microT_CDS/index) predicted that GJB6, SV2B, and SLC12A5 had binding sites with miR-890. Further analysis revealed that miR-890 overexpression had the strongest inhibitory effect on GJB6 expression (Fig. S1C,D), so GJB6 was selected as the target of miR-890 for investigation. The binding sites between miR-890 and circCDR1 or GJB6 were listed in Figure 2A. The results of dual-luciferase reporter assay suggested that miR-890 mimic could specifically reduce the luciferase activities of circCDR1-WT and GJB6-3'UTR-WT vectors, while had not effect on that of their corresponding MUT vectors (Fig. 2B,C). RIP assay showed that the enrichments of circCDR1, miR-890 and GJB6 were significantly enhanced in Anti-Ago2 compared with that in Anti-IgG (Fig. 2D,E). Furthermore, RNA pull-down assay results revealed that circCDR1 enrichment, as well as GJB6 mRNA enrichment, could be increased by the Bio-miR-890-WT vector rather than the Bio-miR-890-MUT vector (Fig. 2F–I). All results showed that circCDR1 could sponge miR-890 and miR-890 could target GJB6.

circCDR1 could sponge miR-890 to regulate GJB6

In glioma tumor tissues, miR-890 expression was upregulated, while the mRNA and protein expression levels of GJB6 were downregulated compared to the normal tissues (Fig. 3A–C). Further analysis showed that miR-890 was negatively correlated with the expression of circCDR1 and GJB6, while circCDR1 was positively correlated with GJB6 mRNA expression in glioma tumor tissues (Fig. 3D–F). Moreover, we found the significantly overexpressed miR-

890 and markedly underexpressed GJB6 (at protein level) in U251 and LN229 cells compared with NHA cells (Fig. 3G,H). To determine the regulatory effects of circCDR1 on miR-890 and GJB6 expression, circCDR1 overexpression vector and miR-890 mimic were constructed. The increased circCDR1 expression and miR-890 expression confirmed the good transfection efficiency of circCDR1 overexpression vector and miR-890 mimic, respectively (Fig. 3I,J). In U251 and LN229 cells co-transfected with circCDR1 overexpression vector and miR-890 mimic, we discovered that overexpressed circCDR1 could remarkably reduce miR-890 level and enhance GJB6 protein level, while these effects could be reversed by miR-890 overexpression (Fig. 3K,L). These data confirmed that

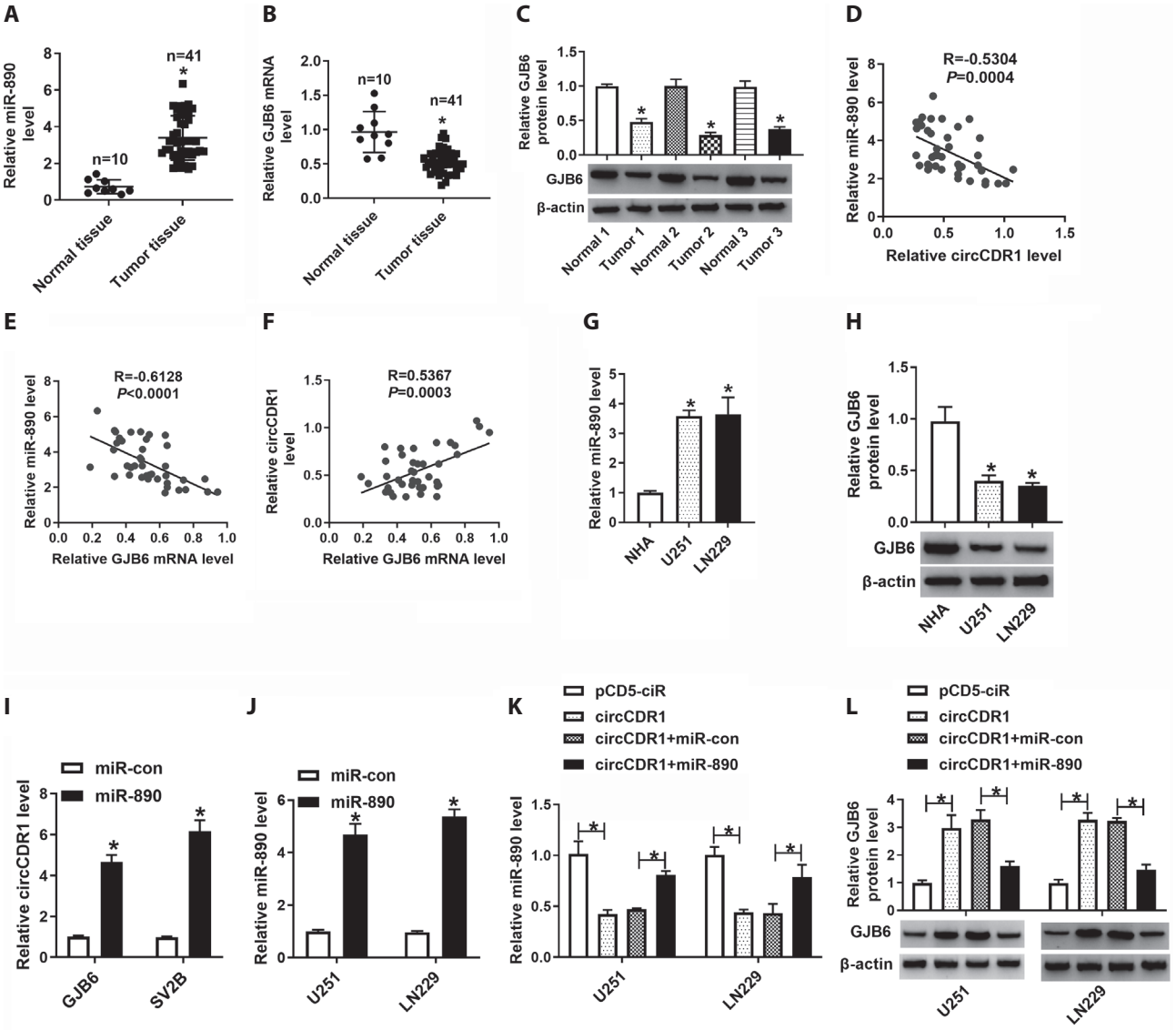

Figure 3. circCDR1 could sponge miR-890 to regulate GJB6. **A.** The miR-890 expression in glioma tumor tissues and normal tissues was measured using qRT-PCR. **B, C.** The mRNA and protein levels of GJB6 were determined by qRT-PCR and WB analysis in glioma tumor tissues and normal tissues. **D–F.** The correlations among circCDR1, miR-890 and GJB6 were analyzed using Pearson correlation analysis. **G, H.** QRT-PCR and WB analysis were performed to determine the miR-890 expression and GJB6 protein expression in glioma cell lines (U251 and LN229) and NHA cells, respectively. **I, J.** The expression of circCDR1 and miR-890 was examined by qRT-PCR to assess the transfection efficiencies of circCDR1 overexpression vector and miR-890 mimic. **K, L.** U251 and LN229 were transfected with pCD5-ciR, circCDR1, circCDR1+miR-con or circCDR1+miR-890. The miR-890 level and GJB6 protein level were determined using qRT-PCR and WB analysis, respectively. A–B, Student's *t*-test; C, G, H, K and L, one-way ANOVA followed by Tukey's *post hoc* test; I–J, two-way ANOVA followed by Tukey's post hoc test. * $p < 0.05$.

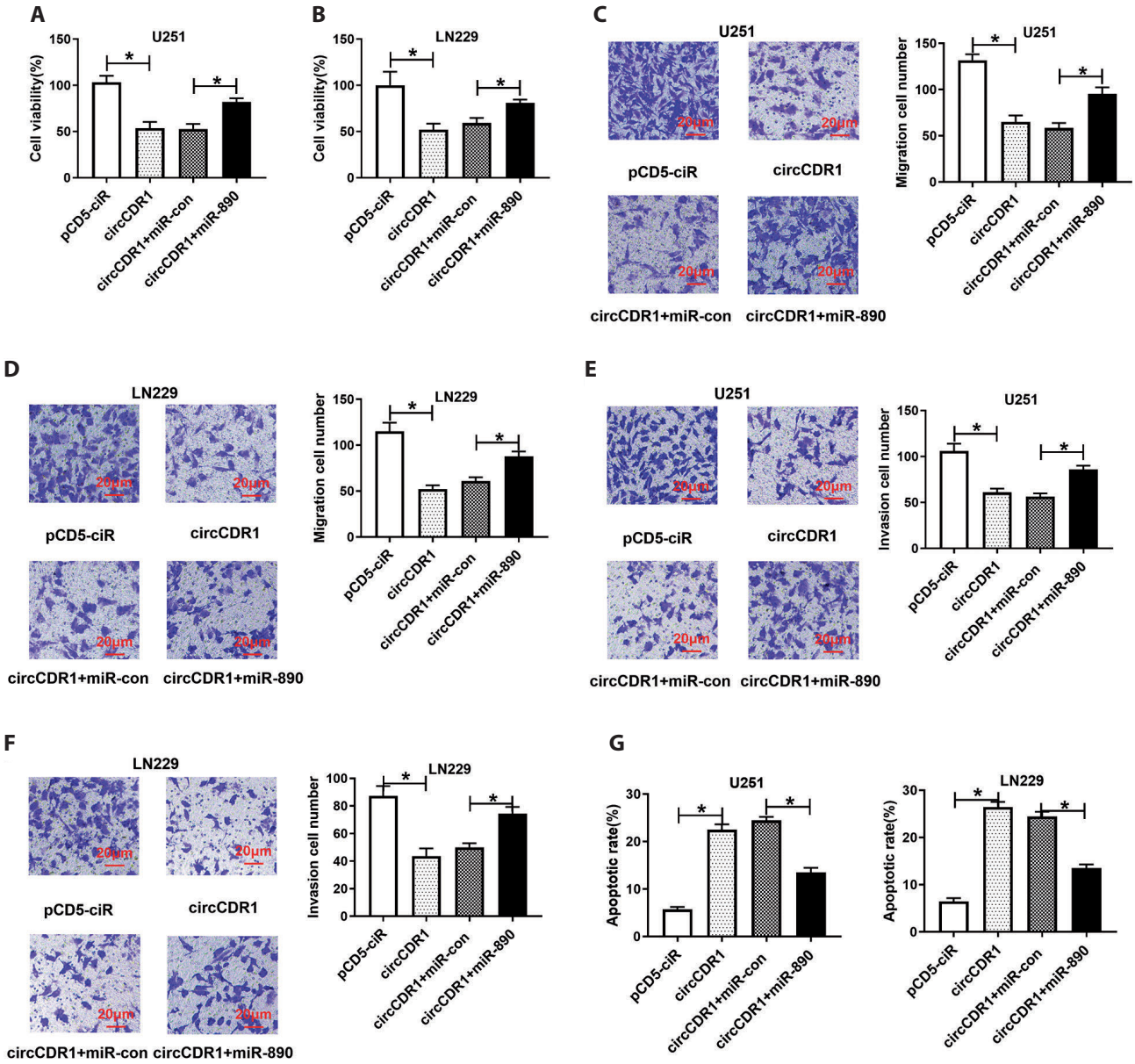

Figure 4. MiR-890 and circCDR1 overexpression regulated glioma cell progression. U251 and LN229 cells were transfected with pCD5-ciR, circCDR1, circCDR1+miR-con or circCDR1+miR-890. Cell viability, migration and invasion cell numbers, and apoptotic rates were determined using CCK8 assay (**A, B**), transwell assay (**C–F**) and flow cytometry (**G, H**), respectively. A–G, one-way ANOVA followed by Tukey's *post hoc* test. * $p < 0.05$.

circCDR1 could serve as a sponge of miR-890 to indirectly regulate GJB6.

MiR-890 reversed the regulation of circCDR1 on glioma cell progression

To confirm that circCDR1 regulated glioma progression by sponging miR-890, we co-transfected with circCDR1 overexpression vector and miR-890 mimic into glioma cells. The results revealed that the inhibition effects of circCDR1 upregulation on the viability, migration, and invasion of U251 and LN229 cells could be reversed by miR-890 overexpression (Fig. 4A–F). Also, the enhancing effect of circCDR1 overexpression on the apoptotic rates of U251 and LN229 cells could be abolished by miR-890 mimic (Fig. 4G,H). Furthermore, circCDR1 overexpression also increased BAX protein level and the decreased Bcl2 protein level, while these effects could be reversed by the overexpression of miR-890 (Fig. S2A–D). Hence, our data showed that circCDR1 sponged miR-890 to inhibit glioma progression.

The inhibition effect of miR-890 inhibitor on glioma progression could be reversed by GJB6 silencing

To further determine whether miR-890 regulated glioma progression by targeting GJB6, the miR-890 inhibitor and the siRNA of GJB6 were built. After transfected them into U251 and LN229 cells, miR-890 expression and GJB6 protein expression were remarkably reduced, respectively (Fig. 5A,B), suggesting that the transfection efficiency of in-miR-890 and si-GJB6 was good, and the subsequent experiments could be carried out. Then, in-miR-890 and si-GJB6 were co-transfected into U251 and LN229 cells. The detection results of GJB6 protein level showed that miR-890 inhibitor could enhance GJB6 expression and this effect could be reversed by GJB6 knockdown in U251 and LN229 cells (Fig. 5C,D). Further experiments indicated that the viability, migration and invasion of U251 and LN229 cells could be repressed by miR-890 inhibitor, while the addition of si-GJB6 could reverse these effects (Fig. 5E–J). By measuring the apoptotic rate and the BAX and BCL2 protein levels, we discovered that knockdown of GJB6 also reversed the promotion effect of miR-890 inhibitor on the apoptosis of U251 and LN229 cells (Fig. 5K,L and Fig. S2E–H). These results indicated that miR-890 targeted GJB6 to regulate glioma progression.

CNPs could contain both TMZ and circCDR1 in glioma cells

Subsequently, we used the interaction of HA and CS to prepare NPs, and further prepared the different drug-loaded NPs (TNPs, circNPs, and CNPs). Under the TEM, we calculate that the diameter of BNPs is 165 ± 18 nm, the diameter of TNPs is greater than BNPs (180 ± 10 nm), the diameter of circNPs is greater than BNPs but no difference can be seen (169 ± 9 nm), and the diameter of CNPs is 203 ± 11 nm (Fig. 6A). Agarose gel electrophoresis analysis showed that naked circCDR1 could move from the negative electrode to the positive electrode in an electric field, while CNPs could stably retain circCDR1 in the gel pores. However, after SDS treatment, circCDR1 could be freed from the gel pores and moved from the negative electrode to the positive electrode (Fig. 6B). These results indicated that CNPs could encapsulate circCDR1 stably, and after competitively binding with NPs through SDS, circCDR1 could be released from CNPs again. Laser confocal microscopy analysis showed that after CNPs were cultured with cells, a large amount of green fluorescence (FAM-circCDR1) and red fluorescence (TMZ) appeared in the cell cytoplasm and the two almost overlapped after merge, which indicated that CNPs could simultaneously transport circCDR1 and TMZ into cells (Fig. 6C,D). After adding HA, the intensity of green fluorescence and red fluorescence in the cells was significantly reduced (Fig. 6C,D), indicating that the HA added in advance had interacted with receptors such as CD44, which weakened the interaction between HA and CD44 in CNPs, thereby reducing the entry ability of CNPs into cells. It could be concluded that CNPs could deliver circCDR1 and TMZ into glioma cells, which was achieved mainly through a phagocytic mechanism mediated by ligand-receptor (HA-CD44).

NPs and TMZ could inhibit the progression of glioma cells

To assess the effect of NPs on glioma cell progression, U251 and LN229 cells were co-cultured with BNPs, TNPs, circNPs and CNPs, or treated with TMZ. Compared to the control group and BNPs group, we found that TMZ treatment and circNPs, TNPs and CNPs co-culture also could inhibit the viability, migration and invasion of U251 and LN229 cells, among which CNPs had the best effect (Fig. 7A–F). In addition, the results of flow cytometry suggested that the apoptotic rate of U251 and LN229 cells could be promoted by TMZ, circNPs, TNPs and CNPs, and the pro-apoptosis ability of CNPs was better (Fig. 7G,H). Also, TMZ, circNPs, TNPs and CNPs could enhance the protein level of BAX and suppress the protein level of BCL2 in U251 and LN229 cells (Fig. S2I–L). These data confirmed that TMZ, circNPs, TNPs and CNPs could inhibit glioma cell proliferation, migration, invasion and promote apoptosis. Among them, CNPs co-delivering TMZ and circCDR1 had the best effect.

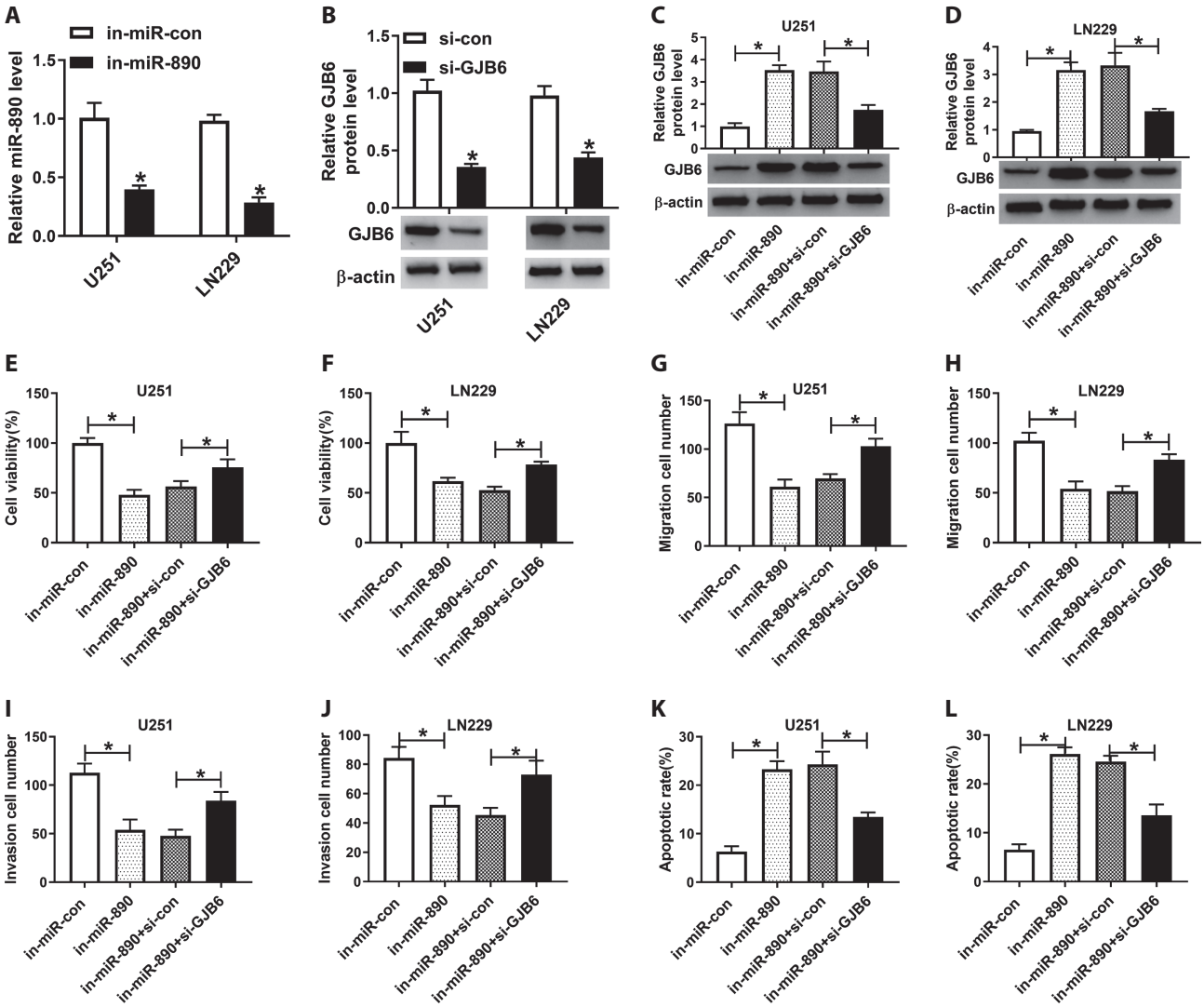

Figure 5. MiR-890 inhibitor and GJB6 silencing regulated glioma progression. **A, B.** The transfection efficiencies of in-miR-890 and si-GJB6 were evaluated by detecting miR-890 level and GJB6 protein level using qRT-PCR and WB analysis, respectively. **C–L.** U251 and LN229 cells were transfected with in-miR-con, in-miR-890, in-miR-890+si-con or in-miR-890+si-GJB6. **C, D.** The protein level of GJB6 was examined using WB analysis. CCK8 assay (**E, F**), transwell assay (**G–J**) and flow cytometry (**K, L**) were utilized for measuring cell viability, migration and invasion cell numbers, and apoptotic rates, respectively. A–B, two-way ANOVA followed by Tukey's *post hoc* test; C–L, one-way ANOVA followed by Tukey's *post hoc* test. * $p < 0.05$.

NPs and TMZ had a strong inhibitory effect on glioma tumor growth in vivo

In addition, we assessed the effects of various types of NPs and TMZ on glioma tumor growth. The results showed that the tumor volume, weight and size of mice in the circNPs, TMZ, TNPs and CNPs groups were significantly lower than the control group, and the effect was more obvious in the CNPs group (Fig. 8A,B). Moreover, significantly high expression of circCDR1 was detected in the tumor tissues of all treatment groups (Fig. 8C), especially in circNPs group and CNPs group, indicating that TMZ and TNPs could promote circCDR1 expression, and the circNPs and CNPs could effectively deliver circCDR1. In addition, we also found the significantly low-expressed miR-890 and high-expressed GJB6 protein in each treatment group (Fig. 8D,E). IHC staining showed that GJB6 positive cells were markedly increased in the tumor tissues of the circNPs, TMZ, TNPs and CNPs treatment groups compared to the control group (Fig. 8F). These results confirmed that the circNPs, TMZ, TNPs and CNPs could regulate the expression of miR-890 and GJB6 to suppress glioma tumor growth, and CNPs had the best effect.

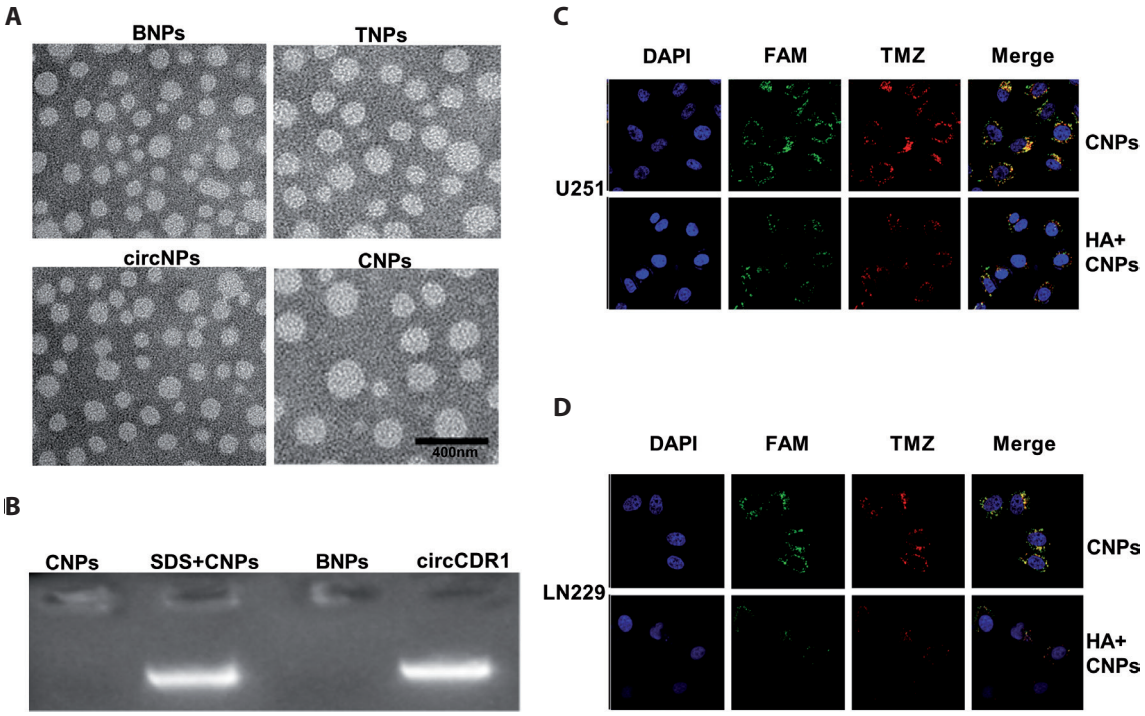

Figure 6. CNPs could contain both TMZ and circCDR1 in glioma cells. **A.** The morphology and size of NPs were observed using TEM. **B.** Agarose gel electrophoresis analysis was used to assess whether circCDR1 encapsulated in CNPs. **C, D.** Laser confocal microscopy images showed the cellular uptake of CNPs in glioma cells.

Discussion

Tumors are abnormal lesions formed by the body under the action of various carcinogenic factors, tissue cells lose normal regulation of their growth at the gene level, leading to abnormal proliferation (Burgio et al. 2018; Lai 2018). The pathogenesis of tumors is complex, and the study of tumor pathogenesis is one of the major issues in medicine. At present, it has been discovered that many circRNAs are involved in the regulation of glioma progression, such as circ_0005114 (Wei et al. 2021), circEZH2 (Wen et al. 2021) and circSCAF11 (Yin et al. 2020). Our study indicated the low expression of circCDR1 in glioma tissues and cells, which was consistent with the results of previous studies (Li and Diao 2019). In addition, we also confirmed that low circCDR1 expression was associated with the poor prognosis of glioma patients. The characteristic that circCDR1 was mainly distributed in the cytoplasm provided the necessary conditions for circCDR1 to be the ceRNA of miRNA.

In order to reveal the underlying molecular mechanism of circCDR1, we conducted bioinformatics analysis and experiments validation, and confirmed that circCDR1 could act as a ceRNA for miR-890 to regulate GJB6. MiR-890 has been shown to be abnormally expressed in many tumors and is closely related to the occurrence and development of tumors, including breast cancer (Wang et al. 2019), melanoma (Xia et al. 2020) and prostate cancer (Pashaei et al. 2017). Wang et al. suggested that miR-890 was upregulated in glioma and could function as a tumor promoter to facilitate glioma progression (Wang et al. 2020). Our study showed that miR-890 was highly expressed in glioma tissues and cells. Further analysis showed that miR-890 reversed the inhibition of circCDR1 on glioma progression, which suggested that circCDR1 sponged miR-890 to hinder glioma progression.

GJB6 (also known as connexin 30), a member of the connexin protein family, is an important channel for maintaining the transport of signal molecules between charged atoms (ions) and adjacent cells (Defourny et al. 2019). In glioma related studies, GJB6 was considered to be a key gene that inhibited glioma progression (Princen et al. 2001; Mennecier et al. 2008; Artesi et al. 2015). Consistent with this, we confirmed that GJB6 was a markedly downregulated gene in glioma through analyzing in GEO database. The rescue experiments determined that GJB6 knockdown could reverse the suppressive effect of miR-890 inhibitor on glioma progression, which once again verified that miR-890 targeted GJB6 to regulate glioma progression. Above all, we proposed that circCDR1 restrained glioma progression by regulating the miR-890/GJB6 axis.

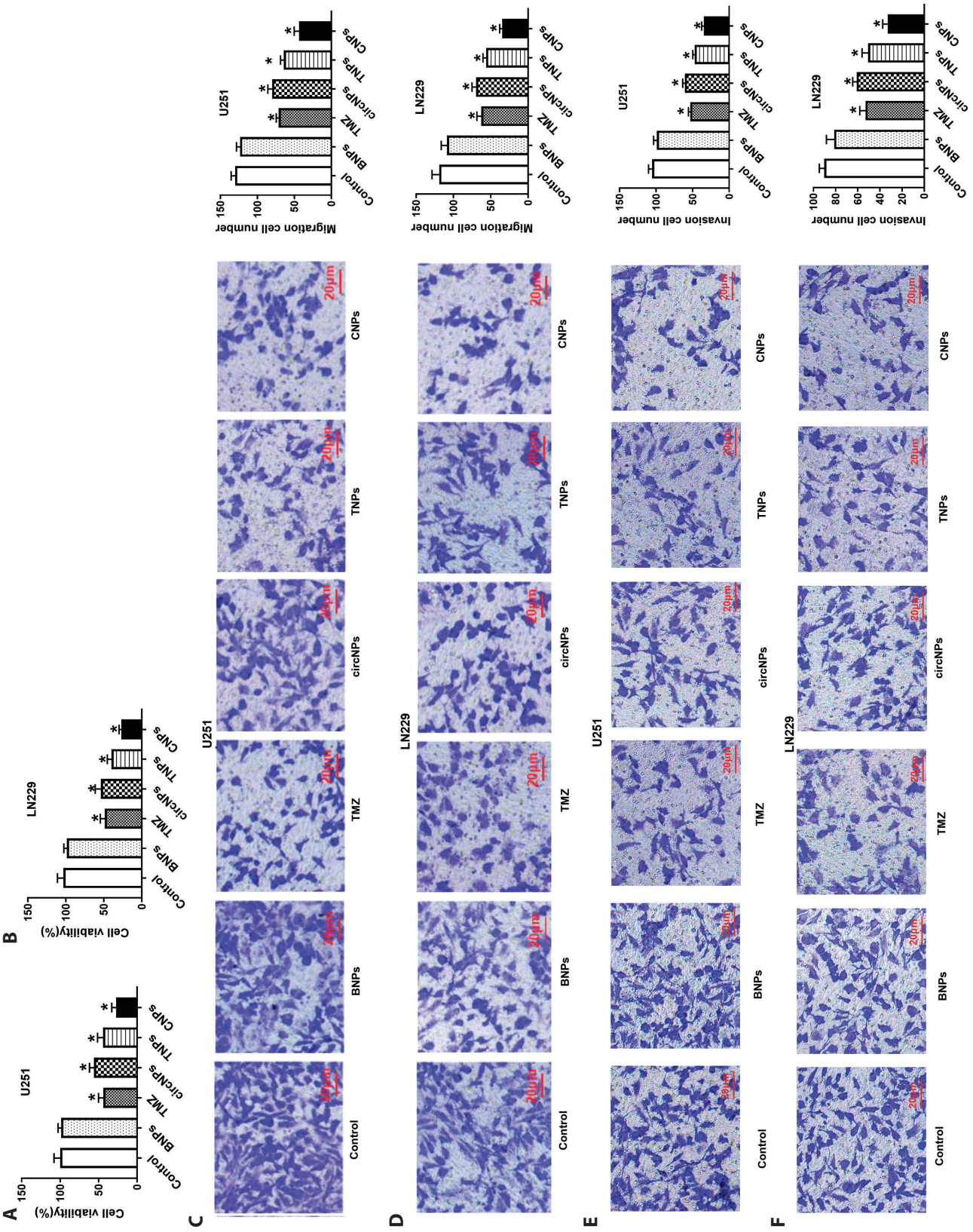
A
U251
Cell viability(%)
150
100
50
0
Control
BNPs
TMZ
circNPs
TNPs
CNPs
B
LN229
Cell viability(%)
C
U251
Control
BNPs
TMZ
circNPs
TNPs
CNPs
Migration cell number
D
LN229
E
U251
Invasion cell number
F
LN229
20μm

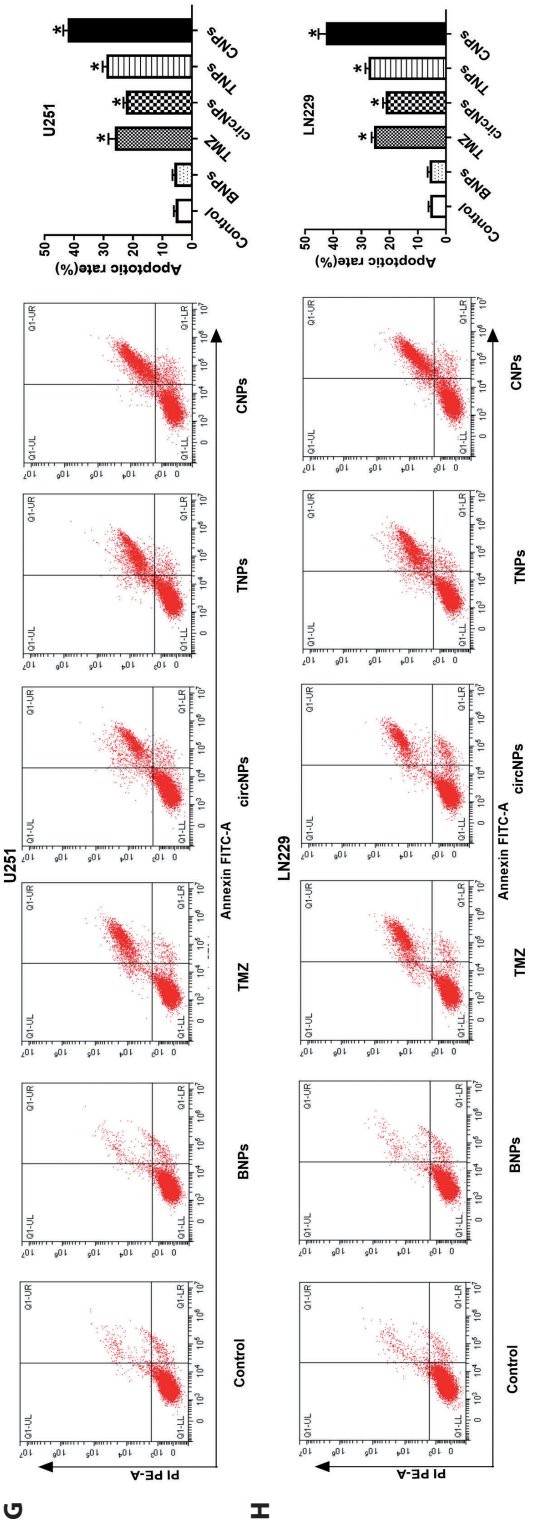

Figure 7. NPs and TMZ could inhibit the progression of glioma cells. U251 and LN229 cells were co-cultured with BNPs, circNPs, TNPs or CNPs, or treated with TMZ. Non-treated cells were used as control. CCK8 assay (**A, B**), transwell assay (**C–F**) and flow cytometry (**G, H**) were used to measure cell viability, migration and invasion cell numbers, and apoptotic rates, respectively. A–H, one-way ANOVA followed by Tukey's *post hoc* test. * $p < 0.05$.

TMZ, a new-generation chemotherapeutic drug, has a good anti-glioma effect. However, the occurrence of TMZ resistance greatly reduces the effectiveness of TMZ in the treatment of glioma (Jiapaer et al. 2018; Karachi et al. 2018). The use of nanotechnology for the collaborative treatment of drugs and genes has become a hot spot in tumor treatment. In this study, we have successfully constructed HA-CS NPs through the interaction between the charges of HA and CS, which had tumor-specific targeting functions. The morphology of the NPs was observed by TEM, and the results showed that the NPs were regular spherical and uniformly dispersed, and the inclusion of TMZ and circCDR1 in CNPs could significantly increase the particle size of the NPs. In addition, we also confirmed that the CNPs could efficiently co-deliver TMZ and circCDR1 into glioma cells. Further experiments showed that TMZ, circNPs, TNPs and CNPs could repress glioma cell viability, migration, invasion, and enhance cell apoptosis *in vitro*, as well as inhibit glioma tumor growth *in vivo*. It was worth noting that both *in vitro* and *in vivo* experiments showed that CNPs had the best inhibitory effect on glioma cell progression and tumor growth. In addition, TMZ treatment could also significantly promote the expression of circCDR1 and GJB6 and inhibit the expression of miR-890, suggesting that TMZ might also inhibit glioma progression by regulating the circCDR1/miR-890/GJB6 axis.

Recent study showed that loading TMZ in hollow manganese dioxide NPs and targeting ligands RAP12 for dual-targeted delivery could synergistically alleviate hypoxia microenvironment and overcome TMZ resistance, further enhancing the anti-tumor effect of chemotherapy against glioblastoma (Chen et al. 2024). Besides, potent and broad-spectrum of the unique nanocomplexes of diethyldithiocarbamate (ALDH1A1 inhibitor) with ferrous oxide NPs could play anti-cancer activities in glioma by inducing iron accumulation-triggered ferroptosis (Abu-Serie et al. 2024). The above information suggests that effective drug and gene nanoparticle co-delivery may have great achievements in the treatment of glioma. Consistent with these study, our data indicated that TMZ and circCDR1 NPs co-delivery system could inhibit glioma cell progression and tumorigenesis, which identified the potential of NPs in glioma therapy. Of course, it is important to explore the pharmacokinetic properties of these nanoparticles to understand their behavior *in vivo*. Unfortunately, due to financial constraints, we have not yet explored the pharmacokinetic properties of these nanoparticles. This is the limitation of our study and will be the direction of our future research. Besides, due to the limitation of funds, we have only carried out agarose gel electrophoresis assay to confirm the nucleic acid loading on NPs. Of course, this is not enough, and we may carry out other experiments in the future to further confirm.

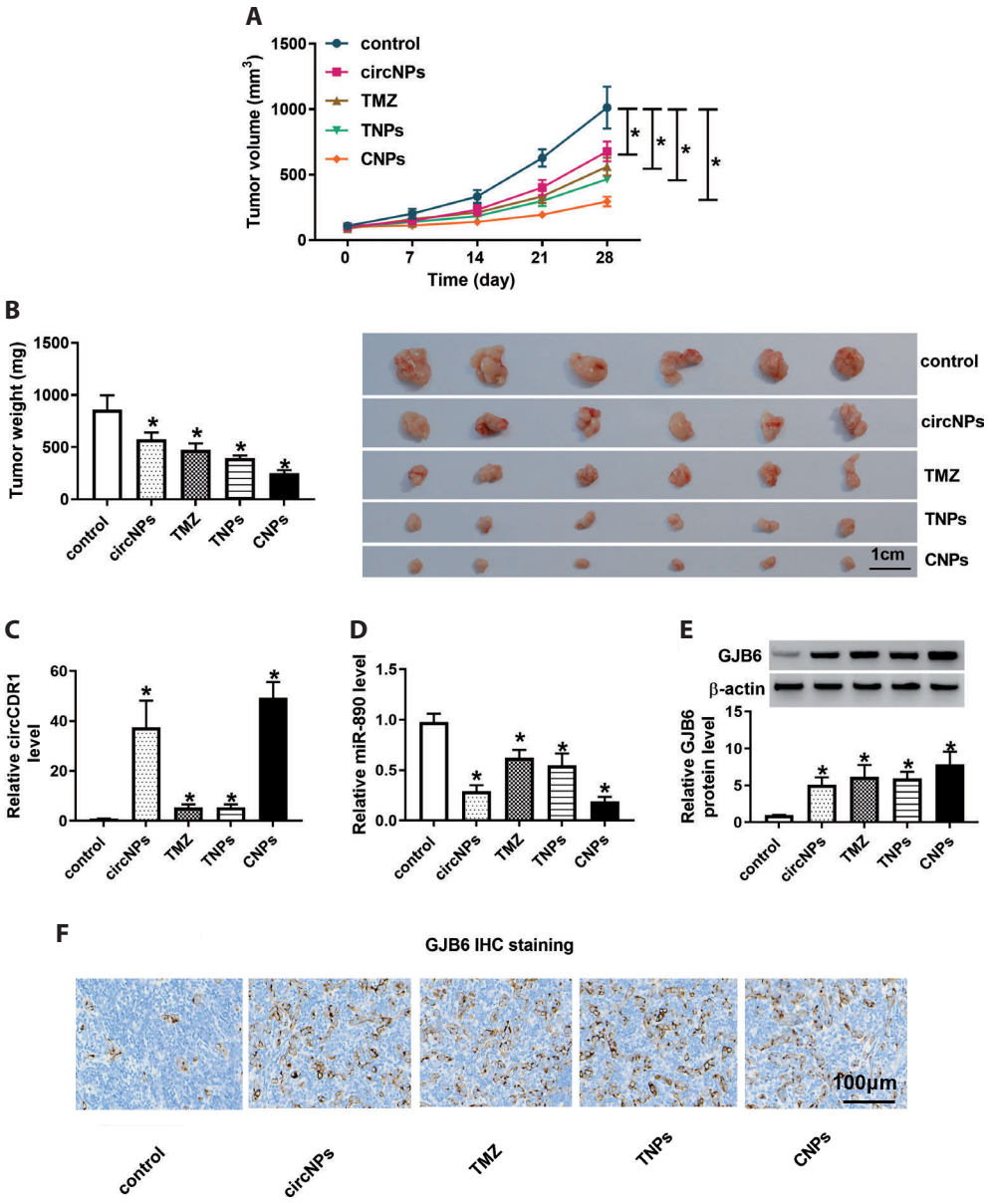

Figure 8. NPs and TMZ could suppress glioma tumor growth *in vivo.* LN229 cells were injected into nude mice, and then circNPs, TMZ, TNPs and CNPs were injected into mice when the tumors grew to 100 mm^3. **A.** Tumor volume was measured every 7 days. **B.** Tumor weight was detected after 28 days and the tumor images of each group were shown. **C, D.** QRT-PCR was used to determine circCDR1 and miR-890 levels in the tumor tissues of each group. **E.** The protein level of GJB6 in the tumor tissues of each group was examined using WB analysis. **F.** The GJB6 IHC staining of tumor tissues in each group was shown. A, two-way ANOVA followed by Tukey's *post hoc* test; B–E, one-way ANOVA followed by Tukey's *post hoc* test. * $p < 0.05$.

In summary, our results showed that circCDR1 could inhibit glioma progression by regulating the miR-890/GJB6 axis, and the TMZ and circCDR1 NPs co-delivery system had better anti-tumor effect in glioma. Our study proposed a new mechanism by which circCDR1 regulated glioma progression and provided a new reference for drug/gene co-therapy for malignant tumor. This study demonstrated that NPs provide a novel approach for the efficient delivery of chemotherapy drugs and targeted gene therapy, which may provide a new idea for the treatment of glioma in the clinic.

Conflict of interest. The authors declare that they have no conflict of interests.

Reference

Abu-Serie MM, Osuka S, Heikal LA, Teleb M, Barakat A, Dudeja V (2024): Diethyldithiocarbamate-ferrous oxide nanoparticles inhibit human and mouse glioblastoma stemness: aldehyde dehydrogenase 1A1 suppression and ferroptosis induction. Front. Pharmacol. **15,** 1363511 https://doi.org/10.3389/fphar.2024.1363511

Almutairi FM, Abd-Rabou AA, Mohamed MS (2019): Raloxifene-encapsulated hyaluronic acid-decorated chitosan nanoparticles selectively induce apoptosis in lung cancer cells. Bioorg. Med. Chem. **27,** 1629-1638 https://doi.org/10.1016/j.bmc.2019.03.004

Artesi M, Kroonen J, Bredel M, Nguyen-Khac M, Deprez M, Schoysman L, Poulet C, Chakravarti A, Kim H, Scholtens D, et al. (2015): Connexin 30 expression inhibits growth of human malignant gliomas but protects them against radiation therapy. Neuro Oncol. **17,** 392-406 https://doi.org/10.1093/neuonc/nou215

Assa F, Jafarizadeh-Malmiri H, Ajamein H, Vaghari H, Anarjan N, Ahmadi O, Berenjian A (2017): Chitosan magnetic nanoparticles for drug delivery systems. Crit. Rev. Biotechnol. **37,** 492-509 https://doi.org/10.1080/07388551.2016.1185389

Barrett SP, Salzman J (2016): Circular RNAs: analysis, expression and potential functions. Development **143,** 1838-1847 https://doi.org/10.1242/dev.128074

Burgio E, Piscitelli P, Colao A (2018): environmental carcinogenesis and transgenerational transmission of carcinogenic risk: From genetics to epigenetics. Int. J. Environ. Res. Public Health **15,** 1791 https://doi.org/10.3390/ijerph15081791

Cai J, Fu J, Li R, Zhang F, Ling G, Zhang P (2019): A potential carrier for anti-tumor targeted delivery-hyaluronic acid nanoparticles. Carbohydr. Polym. **208,** 356-364 https://doi.org/10.1016/j.carbpol.2018.12.074

Chen LL, Yang L (2015): Regulation of circRNA biogenesis. RNA Biol. **12,** 381-388 https://doi.org/10.1080/15476286.2015.1020271

Chen X, Zheng Y, Zhang Q, Chen Q, Chen Z, Wu D (2024): Dual-targeted delivery of temozolomide by multi-responsive nanoplatform via tumor microenvironment modulation for overcoming drug resistance to treat glioblastoma. J. Nanobiotechnology **22,** 264 https://doi.org/10.1186/s12951-024-02531-3

Chiesa E, Dorati R, Conti B, Modena T, Cova E, Meloni F, Genta I (2018): Hyaluronic acid-decorated chitosan nanoparticles for CD44-targeted delivery of everolimus. Int. J. Mol. Sci. **19,** 2310 https://doi.org/10.3390/ijms19082310

Defourny J, Thelen N, Thiry M (2019): Cochlear connexin 30 homomeric and heteromeric channels exhibit distinct assembly mechanisms. Mech. Dev. **155,** 8-14 https://doi.org/10.1016/j.mod.2018.10.001

Deng X, Cao M, Zhang J, Hu K, Yin Z, Zhou Z, Xiao X, Yang Y, Sheng W, Wu Y, et al. (2014): Hyaluronic acid-chitosan nanoparticles for co-delivery of MiR-34a and doxorubicin in therapy against triple negative breast cancer. Biomaterials **35,** 4333-4344 https://doi.org/10.1016/j.biomaterials.2014.02.006

Ferris SP, Hofmann JW, Solomon DA, Perry A (2017): Characterization of gliomas: from morphology to molecules. Virchows Arch. **471,** 257-269 https://doi.org/10.1007/s00428-017-2181-4

Hu X, Wu T, Bao Y, Zhang Z (2017): Nanotechnology based therapeutic modality to boost anti-tumor immunity and collapse tumor defense. J. Control Release **256,** 26-45 https://doi.org/10.1016/j.jconrel.2017.04.026

Jiapaer S, Furuta T, Tanaka S, Kitabayashi T, Nakada M (2018): Potential strategies overcoming the temozolomide resistance for glioblastoma. Neurol. Med. Chir. (Tokyo) **58,** 405-421 https://doi.org/10.2176/nmc.ra.2018-0141

Kang L, Gao Z, Huang W, Jin M, Wang Q (2015): Nanocarrier-mediated co-delivery of chemotherapeutic drugs and gene agents for cancer treatment. Acta Pharm. Sin. B **5,** 169-175 https://doi.org/10.1016/j.apsb.2015.03.001

Karachi A, Dastmalchi F, Mitchell DA, Rahman M (2018): Temozolomide for immunomodulation in the treatment of glioblastoma. Neuro Oncol. **20,** 1566-1572 https://doi.org/10.1093/neuonc/noy072

Lai S (2018): Carcinogenesis is consequence of failure of tissue development. Med. Hypotheses **119,** 84-87 https://doi.org/10.1016/j.mehy.2018.07.025

Li T, Shen X, Geng Y, Chen Z, Li L, Li S, Yang H, Wu C, Zeng H, Liu Y (2016): Folate-functionalized magnetic-mesoporous silica nanoparticles for drug/gene codelivery to potentiate the antitumor efficacy. ACS Appl. Mater. Interfaces **8,** 13748-13758 https://doi.org/10.1021/acsami.6b02963

Li X, Diao H (2019): Circular RNA circ_0001946 acts as a competing endogenous RNA to inhibit glioblastoma progression by modulating miR-671-5p and CDR1. J. Cell. Physiol. **234,** 13807-13819 https://doi.org/10.1002/jcp.28061

Li Z, Ruan Y, Zhang H, Shen Y, Li T, Xiao B (2019): Tumor-suppressive circular RNAs: Mechanisms underlying their suppression of tumor occurrence and use as therapeutic targets. Cancer Sci. **110,** 3630-3638 https://doi.org/10.1111/cas.14211

Lv J, Yang H, Wang X, He R, Ding L, Sun X (2018): Decreased BRMS1L expression is correlated with glioma grade and predicts poor survival in glioblastoma via an invasive phenotype. Cancer Biomark **22,** 311-316 https://doi.org/10.3233/CBM-171019

Mair DB, Ames HM, Li R (2018): Mechanisms of invasion and motility of high-grade gliomas in the brain. Mol. Biol. Cell **29,** 2509-2515 https://doi.org/10.1091/mbc.E18-02-0123

Mennecier G, Derangeon M, Coronas V, Herve JC, Mesnil M (2008): Aberrant expression and localization of connexin43 and connexin30 in a rat glioma cell line. Mol. Carcinog. **47,** 391-401 https://doi.org/10.1002/mc.20393

Ostrom QT, Gittleman H, Stetson L, Virk SM, Barnholtz-Sloan JS (2015): Epidemiology of gliomas. Cancer Treat. Res. **163,** 1-14 https://doi.org/10.1007/978-3-319-12048-5_1

Pashaei E, Pashaei E, Ahmady M, Ozen M, Aydin N (2017): Meta-analysis of miRNA expression profiles for prostate cancer recurrence following radical prostatectomy. PLoS One **12,** e0179543 https://doi.org/10.1371/journal.pone.0179543

Princen F, Robe P, Gros D, Jarry-Guichard T, Gielen J, Merville MP, Bours V (2001): Rat gap junction connexin-30 inhibits proliferation of glioma cell lines. Carcinogenesis **22,** 507-513 https://doi.org/10.1093/carcin/22.3.507

Thomson DW, Dinger ME (2016): Endogenous microRNA sponges: evidence and controversy. Nat. Rev. Genet. **17,** 272-283 https://doi.org/10.1038/nrg.2016.20

Wang C, Xu C, Niu R, Hu G, Gu Z, Zhuang Z (2019): MiR-890 inhibits proliferation and invasion and induces apoptosis in triple-negative breast cancer cells by targeting CD147. BMC Cancer **19,** 577 https://doi.org/10.1186/s12885-019-5796-9

Wang X, Feng H, Dong W, Wang F, Zhang G, Wu J (2020): Hsa_circ_0008225 inhibits tumorigenesis of glioma via sponging miR-890 and promoting ZMYND11 expression. J. Pharmacol. Sci. **143,** 74-82 https://doi.org/10.1016/j.jphs.2020.02.008

Wei B, Wang L, Zhao J (2021): Circular RNA hsa_circ_0005114-miR-142-3p/miR-590-5p-adenomatous polyposis coli protein axis as a potential target for treatment of glioma. Oncol. Lett. **21,** 58 https://doi.org/10.3892/ol.2020.12320

Wen J, Li X, Ding Y, Zheng S, Xiao Y (2021): Lidocaine inhibits glioma cell proliferation, migration and invasion by modulating the circEZH2/miR-181b-5p pathway. Neuroreport **32,** 52-60 https://doi.org/10.1097/WNR.0000000000001560

Xia XQ, Lu WL, Ye YY, Chen J (2020): LINC00662 promotes cell proliferation, migration and invasion of melanoma by sponging miR-890 to upregulate ELK3. Eur. Rev. Med. Pharmacol. Sci. **24,** 8429-8438 http://doi.org/10.26355/eurrev_202008_22640

Yang S, Gao H (2017): Nanoparticles for modulating tumor microenvironment to improve drug delivery and tumor therapy. Pharmacol. Res. **126,** 97-108 https://doi.org/10.1016/j.phrs.2017.05.004

Yin D, Liu L, Shi Z, Zhang L, Yang Y (2020): Ropivacaine inhibits cell proliferation, migration and invasion, whereas induces oxidative stress and cell apoptosis by circSCAF11/miR-145-5p Axis in glioma. Cancer Manag. Res. **12,** 11145-11155 https://doi.org/10.2147/CMAR.S274975

Zang X, Zhao X, Hu H, Qiao M, Deng Y, Chen D (2017): Nanoparticles for tumor immunotherapy. Eur. J. Pharm. Biopharm. **115,** 243-256 https://doi.org/10.1016/j.ejpb.2017.03.013

Zhang E, Xing R, Liu S, Qin Y, Li K, Li P (2019): Advances in chitosan-based nanoparticles for oncotherapy. Carbohydr. Polym. **222,** 115004 https://doi.org/10.1016/j.carbpol.2019.115004

Zhang Y, Yu F, Bao S, Sun J (2019): Systematic characterization of circular RNA-associated CeRNA network identified novel circRNA biomarkers in Alzheimer's disease. Front. Bioeng. Biotechnol. **7,** 222 https://doi.org/10.3389/fbioe.2019.00222

Zhao X, Cai Y, Xu J (2019): Circular RNAs: biogenesis, mechanism, and function in human cancers. Int. J. Mol. Sci. **20,** 3926 https://doi.org/10.3390/ijms20163926

Received: March 12, 2024
Final version accepted: October 4, 2024